

## Ferroelectric strain modulation of antiferromagnetic moments in Ni/NiO ferromagnet/antiferromagnet heterostructures

Yu-Jun Zhang, Jia-Hui Chen, Liang-Liang Li, Jing Ma, Ce-Wen Nan, and Yuan-Hua Lin\*

*State Key Laboratory of New Ceramics and Fine Processing, School of Materials Science and Engineering, Tsinghua University, Beijing 100084, P. R. China*

(Received 18 January 2017; revised manuscript received 10 March 2017; published 15 May 2017)

Electric field manipulation of magnetic properties has attracted a lot of research interest recently in solid-state physics. However, ferroelectric strain modulation of antiferromagnetic (AFM) layer is rarely studied in ferromagnet/antiferromagnet/ferroelectric heterostructures. In this paper, we prepared a Ni/NiO(001) heterostructure on ferroelectric  $\text{Pb}(\text{Mg}_{1/3}\text{Nb}_{2/3})_{0.7}\text{Ti}_{0.3}\text{O}_3(001)$  substrates and observed an out-of-plane electric field modulation of exchange bias and magnetic anisotropy in the Ni layer. The exchange bias was easily eliminated by an electric field cycle, which was due to the AFM domain switching induced by piezoelectric strain in the NiO layer. Synchrotron x ray linear dichroism results confirmed the AFM moment alignment induced by ferroelectric strain as well. Our work showed a promising strategy to manipulate AFM moments and domains, serving the blooming AFM spintronics.

DOI: [10.1103/PhysRevB.95.174420](https://doi.org/10.1103/PhysRevB.95.174420)

### I. INTRODUCTION

Antiferromagnet (AFM)/ferromagnet (FM) interface magnetic coupling has been keeping itself an intriguing topic in solid-state physics after several decades of rapid development of spintronics [1–4]. The AFMs have been introduced into the magnetic recording devices as a pinning layer to stabilize the magnetic moments by exchange-bias (EB) effect in one of the two FM layers and to induce different magnetoresistance states of the devices [5]. Therefore, AFM/FM coupling mechanism has been intensely investigated. Due to the interface exchange interaction with the AFM pinning layer, the FM layer in the vicinity generally possesses a shift of the hysteresis loop or an enhancement of the coercive field.

With the urgent demand of low power consumption and multifunctionality in spintronic devices, multiferroic heterostructures with capability of electric field control of magnetism has become a competitive candidate for low-power-consumption spintronics applications. Multiferroic heterostructures consisting of ferroelectric (FE) and FM components utilize the interfacial magnetoelectric coupling to realize electric field control of magnetism. Meanwhile, electric field modulation of magnetism in FM/AFM EB systems has also attracted a lot of research interest recently [6–16]. A common strategy is to select specific AFM materials whose domain structure or interface spin can be manipulated by electric field. Typical examples are  $\text{BiFeO}_3$  [7,8,11], whose AFM domains are coupled with its FE domains, and  $\text{Cr}_2\text{O}_3$  [14–16], whose AFM domains can be reoriented by simultaneous application of electric field and magnetic field. The EB in these FM/AFM systems can be modulated by switching the interface moments of the AFM layer, which are coupled to the adjacent FM moments. Although this strategy utilizes the significance of AFM layer in the modulation mechanism, it is only observed in limited materials systems. On the other hand, as FE materials can exhibit strong piezoelectric (PE) response, PE strain effect has been proposed to illustrate the magnetoelectric modulation

mechanisms in FM/AFM heterostructures prepared on FE substrates [6,9,10,12,13]. Xue *et al.* [6] and Liu *et al.* [12] have achieved nearly  $180^\circ$  switching of magnetization by a simple way of using PE effect of FE single crystal substrates. Nevertheless, in these reports, the modulation of AFM moments and domains by PE strain is neglected, and the role of AFM layer is just to introduce a unidirectional anisotropy in the heterostructure because the AFM materials they employed have large magnetic anisotropy and the strain modulation upon them is negligible. In addition, the difficulties in the characterization of AFM domains also introduce obstacles for elucidation of the magnetoelectric modulation mechanisms in AFM layers. The PE modulation of AFM moment in FM/AFM heterostructures has not been reported in detail.

Meanwhile, AFM spintronics is taking the latest tide of development in spintronics currently [17–20]. Replacement of FM materials by AFM materials in magnetic recording media brings the stability to magnetic field and eliminates the stray field, which can improve the miniaturization and reliability of spintronics devices. Many works have been focusing on the probable applications of AFM materials in magnonics and spin transport [21–23]. Wadley *et al.* demonstrated a simple way to switch AFM domains by electrical current [24]. In comparison with the mechanism of spin-orbit torque in an AFM material with the special magnetic structure, as they proposed [24], PE switching of AFM materials is simpler in theory and more applicable in most typical AFM systems. Combination of AFM spintronics and multiferroics could also become an attractive topic in modern condensed matter physics. However, the research regarding to PE switching of AFM domain is rare in the literature so far.

To investigate PE modulation of magnetic properties in FM/AFM structures, in this paper we took advantage of PE strain provided by FE substrates and designed a Ni/NiO/ $\text{Pb}(\text{Mg}_{1/3}\text{Nb}_{2/3})_{0.7}\text{Ti}_{0.3}\text{O}_3$  (PMN-PT) heterostructure, in which EB elimination induced by an out-of-plane electric field was observed. Another bare NiO/PMN-PT sample was prepared for x ray linear dichroism (XLD) measurements to directly study the PE strain effect upon AFM NiO moments. It was confirmed that the electric field induced EB elimination

\*Corresponding author: [linyh@mail.tsinghua.edu.cn](mailto:linyh@mail.tsinghua.edu.cn)

is related to the AFM domain switching of NiO. Meanwhile, the modulation of the magnetic anisotropy in the Ni FM layer was also observed, which could be attributed to 109° FE domain switching of the underneath PMN-PT substrate.

**II. METHODS**

The NiO layer was deposited on PMN-PT(001) single crystal substrate by pulsed laser deposition (PLD), utilizing a KrF excimer pulsed laser ( $\lambda = 248 \text{ nm}$ ) with a repetition rate of 5 Hz and an energy density of  $\sim 1.4 \text{ J/cm}^2$ . The deposition temperature and oxygen pressure were controlled at 650 °C and 50 mTorr, respectively. The distance between the NiO target and the substrate was 8 cm. The growth rate of NiO thin films was  $\sim 0.8 \text{ nm/min}$ . After the NiO deposition, the sample was directly transferred into a magnetron-sputtering chamber with a background vacuum of  $3 \times 10^{-7}$  Torr to deposit Ni. The deposition power of Ni was set at 45 W, and the substrate temperature was 300 °C, resulting in a growth rate of 1.5 nm/min. An external growth field of  $\sim 300 \text{ Oe}$  generated by two parallel arranged permanent magnets was applied in the in-plane [110] direction of the PMN-PT(001) substrate. After the Ni deposition, the samples were cooled down in high vacuum and a 2 nm Pt capping layer was grown at room temperature with a dc (Direct Current) power of 10 W to prevent oxidation of Ni. Gold electrodes with a thickness

of 100 nm were sputtered on the back of the substrate for the Ni (20 nm)/NiO (10 nm)/PMN-PT(001) heterostructure (substrate size: 5 mm length, 5 mm width, 0.5 mm thickness) or on two sides parallel to the (110) crystal plane of the substrate for the NiO (10 nm)/PMN-PT(001) heterostructure (substrate size: 2 mm length, 2 mm width, 1 mm thickness).

A Rigaku SMARTLAB x ray diffractometer (XRD) with Cu  $K\alpha$  radiation was employed to characterize the phase composition and epitaxial relationship. The Magneto-optic Kerr Effect (MOKE, NanoMOKE2, Quantum Design) was employed to characterize the magnetic properties. The MOKE system utilized a 633 nm red laser with a spot size of  $\sim 5 \mu\text{m}$ . The  $M-H$  loops were measured by MOKE after a stabilization time of 30 s following the application of every dc voltage. Polarization-electric field ( $P-E$ ) field loops were measured at a frequency of 10 Hz by a Premier II FE test system (Radiant Technologies, Inc.). The dc voltage was applied by a Keithley 2410 voltage source. Soft XLD spectra were performed at the Beamline BL08U1A of Shanghai Synchrotron Radiation Facility by total electron yield (TEY) mode.

**III. RESULTS**

Figure 1(a) displays the schematic of the sample structure and the MOKE measurement geometry for the Ni/NiO/PMN-PT(001) sample. The voltage was applied between the Ni layer

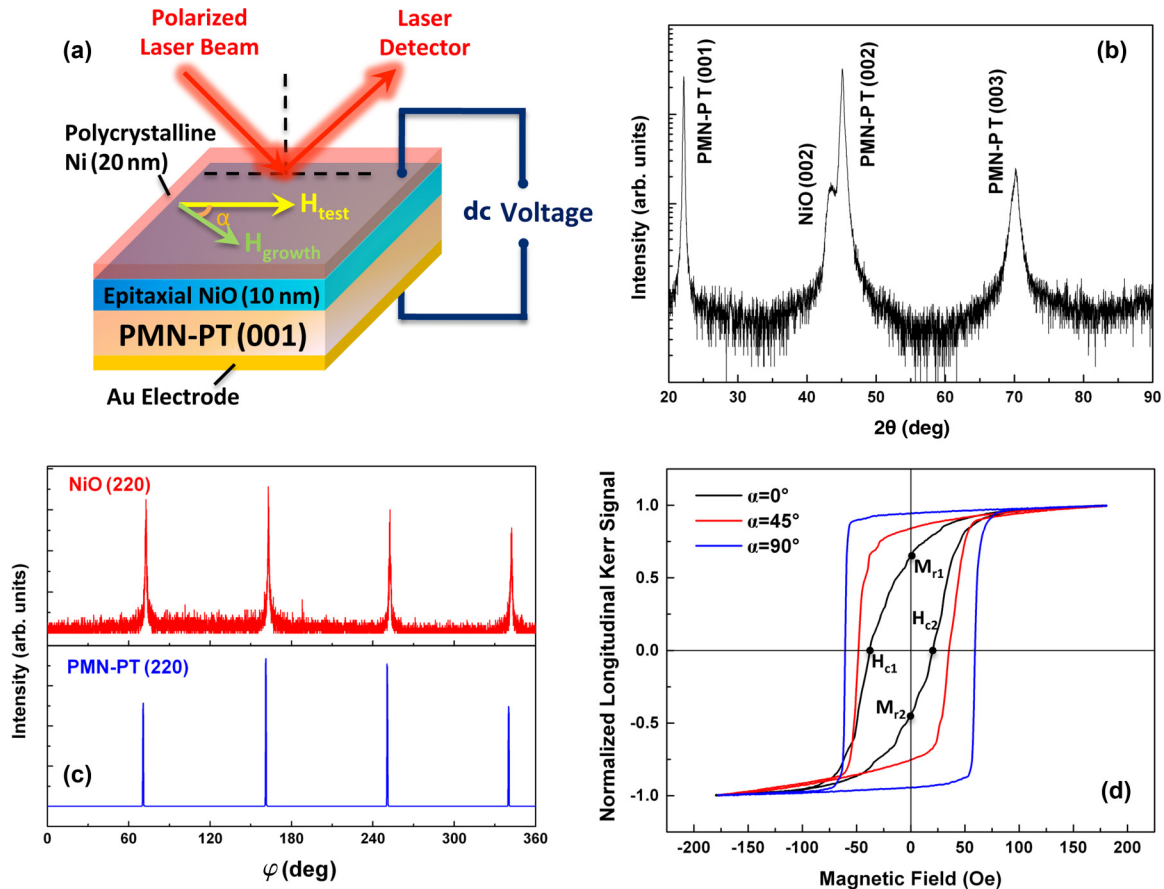


FIG. 1. (a) Schematic diagram of the sample structure and MOKE measurement geometry. (b)  $\theta-2\theta$  scan and (c)  $\varphi$ -scan XRD patterns of the Ni (20 nm)/NiO (10 nm)/PMN-PT(001) heterostructure. (d) Normalized anisotropic  $M-H$  loops of the as-deposited Ni (20 nm)/NiO (10 nm)/PMN-PT(001) heterostructure measured by MOKE.

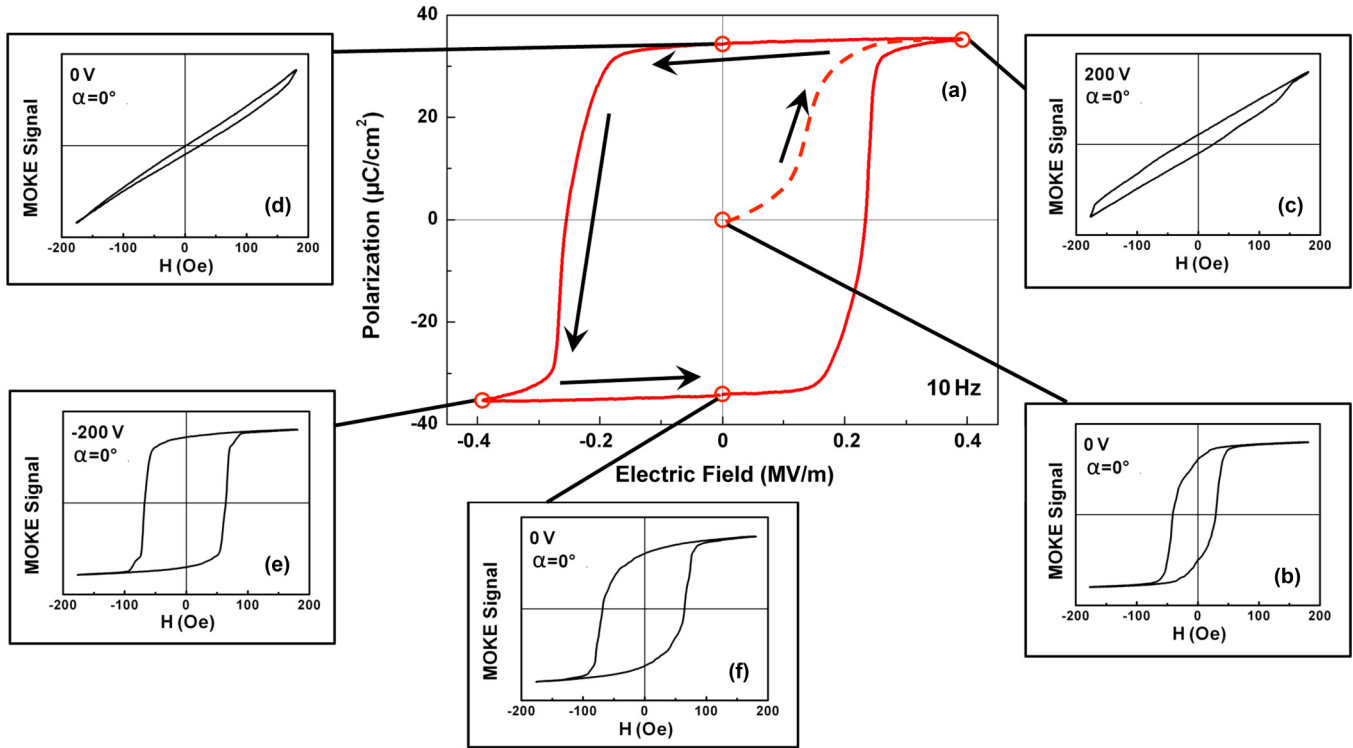


FIG. 2. (a)  $P$ - $E$  loop of the Ni (20 nm)/NiO (10 nm)/PMN-PT(001) heterostructure. The dashed line schematically shows the poling process starting from the as-deposited state. (b)–(e)  $M$ - $H$  loops corresponding to different applied dc voltages in the first voltage cycle. The loops were measured in the in-plane [110] direction.

and the gold bottom electrode. The MOKE measurement was carried out in a longitudinal geometry with an in-plane magnetic field parallel to the incidence plane. The angle between the measurement field and the growth field, namely in-plane [110] direction of the substrate, was defined as  $\alpha$ . Epitaxial growth with corresponding cubic cells ( $[001]_{\text{NiO}}//[001]_{\text{PMN-PT}}$ ,  $[010]_{\text{NiO}}//[010]_{\text{PMN-PT}}$ ,  $[100]_{\text{NiO}}//[100]_{\text{PMN-PT}}$ ) was confirmed by the  $\theta$ - $2\theta$  XRD pattern in Fig. 1(b) and the  $\varphi$ -scan spectra in Fig. 1(c). The Ni layer was not textured and did not appear in the  $\theta$ - $2\theta$  scan. Figure 1(d) shows the anisotropic  $M$ - $H$  loops of the Ni layer. In the  $\alpha = 0^\circ$  direction, an obvious EB effect was observed due to cooling in the growth field from above the Neel temperature of NiO.

Next, we will focus on the  $\alpha = 0^\circ$  direction and apply voltage cycles on the substrate to investigate the manipulation of the magnetic properties by FE strain effects. Figure 2 shows the evolution process of the  $M$ - $H$  loop at  $\alpha = 0^\circ$  in the first dc voltage cycle. As demonstrated in Fig. 2(a), the PMN-PT(001) substrate exhibits a typical FE  $P$ - $E$  loop with a coercive voltage of  $\sim 120$  V. A few  $M$ - $H$  loops corresponding to different applied dc voltages are picked out and shown in Figs. 2(b)–2(f). The as-deposited state [Fig. 2(b)] clearly exhibits an EB induced by the growth field. Consequent application of a positive dc voltage beyond the coercive voltage induces a large nonvolatile change of the magnetic anisotropy, and the  $M$ - $H$  loops show typical hard-axis characters [Figs. 2(c) and 2(d)]. In Figs. 2(e) and 2(f), an applied negative dc voltage beyond the coercive voltage of the PMN-PT substrate switches the  $M$ - $H$  loops back to a shape with higher squareness. It is interesting to

find that the EB was easily eliminated and that an enhancement of the coercive field occurred.

To further analyze the magnetic property modulation by the applied dc voltage, coercive field  $H_c$ , EB field  $H_{\text{eb}}$ , and the normalized remanent magnetization  $M_r$  of the Ni/NiO/PMN-PT(001) heterostructure versus the applied voltage are displayed in Figs. 3(a) and 3(b).  $H_c$ ,  $H_{\text{eb}}$ , and  $M_r$  are defined as  $(|H_{c1}| + |H_{c2}|)/2$ ,  $(H_{c1} + H_{c2})/2$ , and  $(|M_{r1}| + |M_{r2}|)/2$ , respectively.  $H_{c1}$ ,  $H_{c2}$ ,  $M_{r1}$ , and  $M_{r2}$  are picked, as in Fig. 1(d). The evolution processes of the corresponding magnetic parameters of the Ni (20 nm)/PMN-PT(001) heterostructure are displayed in Figs. 3(c) and 3(d) for comparison, which reflects the PE strain effect directly applied upon the Ni layer. It is obvious that the local magnetic properties in the Ni/NiO/PMN-PT(001) heterostructure undergo drastic changes in the first dc voltage cycle. After the EB elimination in the first cycle, the  $H_c$  and  $M_r$  tend to switch between two magnetic anisotropy states without EB (easy-axis state:  $H_c \sim 85$  Oe,  $M_r \sim 0.93$ ; hard-axis state:  $H_c \sim 70$  Oe,  $M_r \sim 0.6$ ), as the Ni/PMN-PT(001) heterostructure does from the first cycle (easy-axis state:  $H_c \sim 45$  Oe,  $M_r \sim 0.6$ ; hard-axis state:  $H_c \sim 30$  Oe,  $M_r \sim 0.3$ ). The  $H_c$  of the Ni/NiO/PMN-PT(001) heterostructure is higher than that of the Ni/PMN-PT(001) heterostructure, indicating a coercive field enhancement effect of the NiO layer. More importantly, the local EB in the first dc voltage cycle changes dramatically from negative to positive and then disappears in the following cycles. This irreversible change of the EB cannot be interpreted without the electric field modulation of the NiO moments. Therefore,

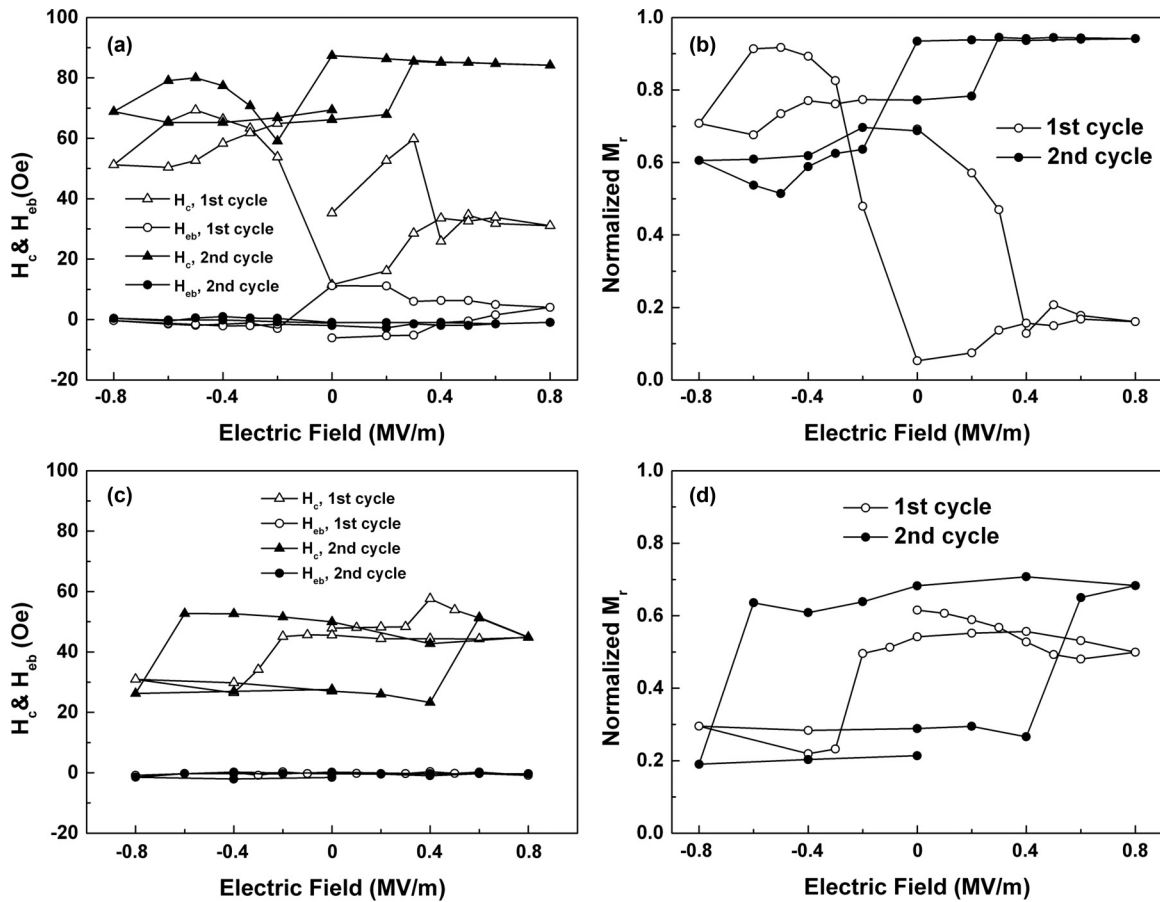


FIG. 3. (a), (b) Evolution of the  $H_{cb}$ ,  $H_c$ , and  $M_r$  of the Ni (20 nm)/NiO (10 nm)/PMN-PT(001) heterostructure in the in-plane [110] direction, which are obtained from the  $M$ - $H$  loops in the in-plane [110] direction. The voltage sequence is from 0 V, 400 V, 0 V, -400 V, to 0 V. (c), (d) The evolution processes of the  $H_{cb}$ ,  $H_c$ , and  $M_r$  for the Ni (20 nm)/PMN-PT(001) heterostructure.

it is necessary to investigate PE strain effect on AFM layer separately.

To confirm the PE-induced AFM moment switching in NiO layer, we used a bare NiO/PMN-PT(001) sample without Ni capping and employed XLD measurement to characterize the AFM spin texture of the NiO layer after aligning the FE domains with in-plane anisotropic strain. In this sample, we

can study the strain effect on AFM layer without the influence of FM Ni moments. Moreover, the NiO surface needs to be exposed to the vacuum during measurement due to the limited detection depth in the TEY mode of XLD. Therefore, we deposited electrodes parallel to the (110) crystal plane on two side faces of the substrate and applied an in-plane electric field to induce FE domain switching. Before the

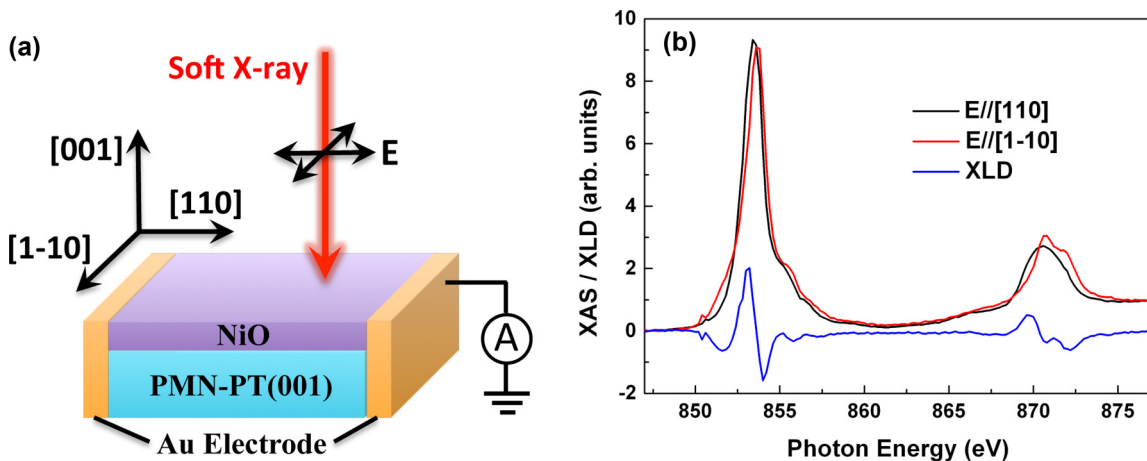


FIG. 4. (a) Schematic of the XLD measurement geometry for an in-plane poled NiO (10 nm)/PMN-PT(001) heterostructure. (b) The XLD spectrum and XAS spectra with  $E//[110]$  and  $E//[1-10]$  of the in-plane poled NiO (10 nm)/PMN-PT(001) heterostructure.

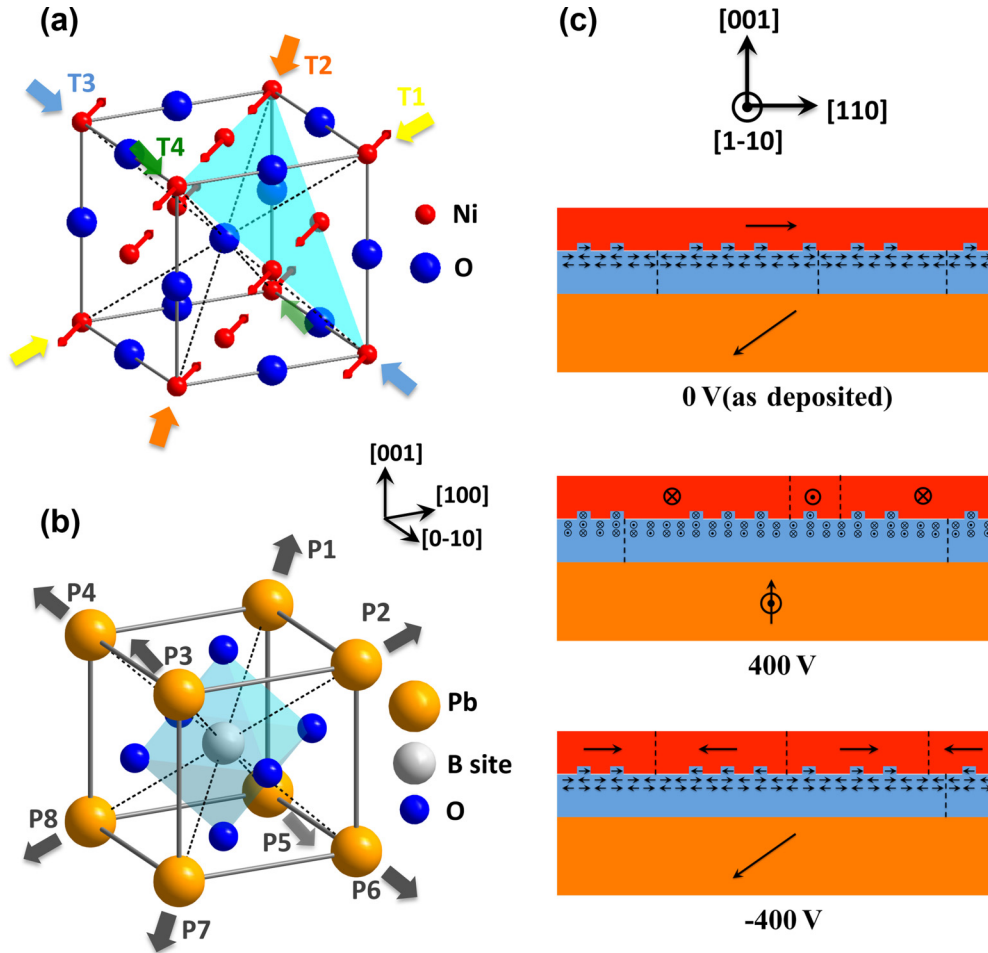


FIG. 5. (a) Schematic of the spin arrangement and domain structure of NiO. The T domains labeled as T1 to T4 have different exchange striction along distinct  $\{111\}$  directions, which is displayed as pairs of arrows with different colors. (b) Schematic of eight possible polarization directions of rhombohedral PMN-PT substrate, which is labeled as P1 to P8. The atoms of Nb, Mg, or Ti occupy the B sites of the perovskite lattice. (c) Possible domain evolution process in the Ni/NiO/PMN-PT heterostructure with a voltage sequence of  $0\text{ V} \sim 400\text{ V} \sim -400\text{ V}$ . The directions of Ni ion spins in the NiO layer are schematically displayed in detail, while only magnetization directions within a ferromagnetic domain in the Ni layer are displayed. Note that the AFM domain walls displayed by dashed lines are only a representation but not corresponding to T domain walls described in the article. The FE polarization in the upper and lower images corresponds to the P7 domain, while the FE polarization in the middle image corresponds to the P2 domain.

XLD measurement, the substrate was poled by applying a  $0.25\text{ MV/m}$  electric field between two gold electrodes. As displayed in Fig. 4(a), the linearly polarized soft x ray with an electric field component  $E$  parallel to  $[110]$  or  $[1-10]$  was perpendicularly incident to the sample surface, and two distinct x ray absorption spectra (XAS) were obtained. The XLD signal is defined as  $\text{XLD} = \text{XAS}(E//[110]) - \text{XAS}(E//[1-10])$ . In the unpoled NiO/PMN-PT(001) heterostructure, the  $[110]$  and  $[1-10]$  directions are identical in crystallography, and the FE domain size ( $\sim 1\text{ }\mu\text{m}$ ) is much smaller than the x ray beam spot size (around  $200 \times 200\text{ }\mu\text{m}^2$ ). So no XLD signal should be expected. However, in the poled sample, the XLD signal was observed, with characteristic positive peaks at  $853.2\text{ eV}$  and  $869.6\text{ eV}$  and negative peaks at  $854\text{ eV}$  and  $872.2\text{ eV}$  [Fig. 4(b)]. The XLD result indicates that the AFM moments of NiO are preferentially aligned parallel to  $[110]$  direction by the applied electric field, according to the reported angle-dependent XLD investigation on NiO [25]. (In Ref. [25], the  $\varepsilon = \mu = 45^\circ$  spectrum in the second panel

of Fig. 3 should correspond to the negative value of XLD signal with our measurement geometry if the NiO moments are aligned along  $[110]$  in our sample.) The in-plane electric field can cause  $71^\circ$  or  $109^\circ$  FE domain switching with a similar in-plane strain as the out-of-plane  $109^\circ$  FE domain switching does, which will be discussed in detail below.

#### IV. DISCUSSIONS

With the results above, we can discuss the mechanism behind the elimination of the local EB. NiO is a typical AFM transition metal oxide with complex magnetic anisotropy and domain structure, which has already been intensely investigated [26–31]. Dipole-dipole interaction dominates the magnetic anisotropy in NiO [32] and induces magnetic easy plane, namely  $\{111\}$  crystal plane group [blue plane in Fig. 5(a)]. The Ni magnetic moments are lying within these planes and coupling with each other ferromagnetically. With AFM superexchange interaction along the  $\langle 001 \rangle$  directions, the

Ni moments are antiferromagnetically arranged in alternative {111} crystal planes [Fig. 5(a)]. The {111} groups of easy planes are accompanied with concomitant lattice contraction along  $\langle 111 \rangle$  directions [29]. Four equivalent twin-domains (T domains) with contraction in different  $\langle 111 \rangle$  directions are schematically illustrated in Fig. 5(a) as T1 to T4 domains. Much weaker anisotropy will further lead to spin-domain (S domains) structures within the easy planes, which will not be discussed here.

With the confirmed epitaxial relationship between the NiO film and the PMN-PT(001) substrate, the FE strain will be effectively transferred to the NiO layer. The rhombohedral PMN-PT substrate has polarization directing eight equivalent  $\langle 111 \rangle$  directions (P1-P8), accompanied with lattice elongation along the polarization directions [Fig. 5(b)]. For the domains with polarizations P1, P3, P5, and P7, an in-plane tensile strain along the [110] direction can be applied to the NiO film. For the P2, P4, P6, and P8 domains, the in-plane tensile strain is in the [1-10] direction. Taking the lattice contraction of different T domains in NiO into account, the in-plane tensile strain along [110] or [1-10] will prefer T1/T3 or T2/T4 domains, respectively. Due to surface anisotropy [33] or exchange coupling with in-plane magnetic moments [34], the NiO AFM moments should be lying parallel to the in-plane [110] direction for T2 or T4 domains, as displayed in Fig. 5(a) or [1-10] direction for T1 or T3 domains in both Ni/NiO/PMN-PT(001) and NiO/PMN-PT(001) samples. An in-plane electric field in the [110] direction can cause either  $71^\circ$  (e.g., from P2 to P1) or  $109^\circ$  (e.g., from P4 to P5) FE domain switching; induce more P1, P3, P5, and P7 domains; and switch the T domains in the adjacent NiO layer to make T2 and T4 domains preferred. Thus, it can be concluded that our XLD results are consistent with the above analysis that the FE strain in the in-plane [110] direction can reorient the AFM moments in the NiO layer and align them parallel to [110]. It is worth noting that an out-of-plane electric field is also capable of causing similar AFM domain switching when a  $109^\circ$  FE domain switching occurs (e.g., from P7 to P2) in the Ni/NiO/PMN-PT(001) heterostructure.

Next, we would like to discuss the mechanism that the EB is eliminated by the PE strain, as schematically shown in Fig. 5(c). On account of the compensated nature of the ideal NiO (001) plane with equal numbers of oppositely aligned moments, the main origin of EB is reported to be the exchange coupling between the FM magnetization and the net NiO interfacial moments induced by interface roughness [35]. During the Ni deposition, the field cooling could induce EB by producing AFM domain walls in the NiO layer to obtain maximum interface net moments parallel to the Ni layer magnetization. The upper image in Fig. 5(c) shows an example of the Ni/NiO heterostructure originally on a P7 domain. The interface net moments are well aligned parallel to the direction of EB, namely in-plane [110], with a preferred T1/T3 AFM domain structure. If a  $109^\circ$  FE domain switching

occurs and the local polarization is switched from P7 to P2 [the middle picture of Fig. 5(c)], the NiO layer will switch to T2/T4 AFM domains with spins parallel to the [1-10] direction in response to the FE strain. Some irreversible AFM domain wall motion may take place in this procedure, and ferromagnetic domain walls will also be rearranged. In the first voltage cycle, the emergent positive EB may be due to perpendicular coupling between FM magnetization and canted AFM interfacial moments [36,37]. Because positive exchange could likely emerge from the perpendicular configuration between strain-aligned NiO moments and measurement-field aligned Ni moments, as in the example in Fig. 5(c), in which NiO moments are aligned parallel to [1-10] and measurement field remains in [110]. And the modulation of  $M$ - $H$  loop squareness should be attributed to in-plane anisotropic strain induced by  $109^\circ$  FE domain switching of the underneath PMN-PT substrate [38]. When the voltage cycle proceeds to a negative value, the AFM domains will again be rearranged, and the originally preferentially arranged interface net moments will be disrupted if the local polarization switches back from P2 to P7. Then, the local coupling between interface net moments and ferromagnetic moments cancels out, resulting in a coercive field enhancement instead of the EB, as shown in the lower picture of Fig. 5(c). Considering various other routes of FE switching, it is worth mentioning that Fig. 5(c) does not represent every possible switching process in our samples but only demonstrates how strain can typically affect the AFM domains and induce the EB elimination. In real samples, any FE switching induced local strain could contribute to the switching of adjacent AFM domains, disrupting the aligned AFM interface net moments and suppressing the local EB.

## V. CONCLUSION

In summary, we observed the EB elimination induced by electric field in the Ni/NiO/PMN-PT multiferroic heterostructure, which could be attributed to the FE strain induced AFM domain switching or domain wall motion. Hence, the strain modulation of the AFM pinning layers in the strain coupled multiferroic heterostructures should be seriously taken into account. On the other hand, the idea of PE manipulation of AFM materials with ultralow power consumption could infuse fresh blood into the prospering AFM spintronics as well.

## ACKNOWLEDGMENTS

This paper was financially supported by National Key Research Programme of China (Grant No. 2016YFA0201003), National Key Project of Research and Development Plan of China (Grant No. 2016YFA0300103), and National Science Foundation of China (Grants No. 51328203, No. 51332001, and No. 51532003). We are also grateful for the discussion and support provided by the staff of Beamline BL08U1A of Shanghai Synchrotron Radiation Facility.

[1] Z. Liu, M. D. Biegalski, S. L. Hsu, S. Shang, C. Marker, J. Liu, L. Li, L. Fan, T. L. Meyer, A. T. Wong, J. A. Nichols, D. Chen, L. You, Z. Chen, K. Wang, K. Wang,

T. Z. Ward, Z. Gai, H. N. Lee, A. S. Sefat, V. Lauter, Z. K. Liu, and H. M. Christen, *Adv. Mater.* **28**, 118 (2016).

- [2] A. Fraile Rodriguez, A. C. Basaran, R. Morales, M. Kovylyna, J. Llobet, X. Borrise, M. A. Marcus, A. Scholl, I. K. Schuller, X. Batlle, and A. Labarta, *Phys. Rev. B* **92**, 174417 (2015).
- [3] M. Gruber, F. Ibrahim, S. Boukari, H. Isshiki, L. Joly, M. Peter, M. Studniarek, V. D. Costa, H. Jabbar, V. Davesne, U. Halisdemir, J. Chen, J. Arabski, E. Otero, F. Choueikani, K. Chen, P. Ohresser, W. Wulfhekel, F. Scheurer, W. Weber, M. Alouani, E. Beaurepaire, and M. Bowen, *Nat. Mater.* **14**, 981 (2015).
- [4] Y. Fan, K. J. Smith, G. Lupke, A. T. Hanbicki, R. Goswami, C. H. Li, H. B. Zhao, and B. T. Jonker, *Nat. Nanotechnol.* **8**, 438 (2013).
- [5] A. E. Berkowitz and K. Takano, *J. Magn. Magn. Mater.* **200**, 552 (1999).
- [6] X. Xue, Z. Zhou, B. Peng, M. Zhu, Y. Zhang, W. Ren, T. Ren, X. Yang, T. Nan, N. X. Sun, and M. Liu, *Sci. Rep.* **5**, 16480 (2015).
- [7] S. M. Wu, S. A. Cybart, P. Yu, M. D. Rossell, J. X. Zhang, R. Ramesh, and R. C. Dynes, *Nat. Mater.* **9**, 756 (2010).
- [8] S. M. Wu, S. A. Cybart, D. Yi, J. M. Parker, R. Ramesh, and R. C. Dynes, *Phys. Rev. Lett.* **110**, 067202 (2013).
- [9] S. Rizwan, S. I. Ali, Q. T. Zhang, S. Zhang, Y. G. Zhao, M. Anis-ur-Rehman, M. Tufail, and X. F. Han, *J. Appl. Phys.* **114**, 104108 (2013).
- [10] S. Polisetty, W. Echtenkamp, K. Jones, X. He, S. Sahoo, and C. Binek, *Phys. Rev. B* **82**, 134419 (2010).
- [11] L. W. Martin, Y. H. Chu, M. B. Holcomb, M. Huijben, P. Yu, S. J. Han, D. Lee, S. X. Wang, and R. Ramesh, *Nano Lett.* **8**, 2050 (2008).
- [12] M. Liu, J. Lou, S. D. Li, and N. X. Sun, *Adv. Funct. Mater.* **21**, 2593 (2011).
- [13] G. A. Lebedev, B. Viala, T. Lafont, D. I. Zakharov, O. Cugat, and J. Delamare, *Appl. Phys. Lett.* **99**, 232502 (2011).
- [14] X. He, Y. Wang, N. Wu, A. N. Caruso, E. Vescovo, K. D. Belashchenko, P. A. Dowben, and C. Binek, *Nat. Mater.* **9**, 579 (2010).
- [15] P. Borisov, A. Hochstrat, X. Chen, W. Kleemann, and C. Binek, *Phys. Rev. Lett.* **94**, 117203 (2005).
- [16] T. Ashida, M. Oida, N. Shimomura, T. Nozaki, T. Shibata, and M. Sahashi, *Appl. Phys. Lett.* **104**, 152409 (2014).
- [17] T. Jungwirth, X. Marti, P. Wadley, and J. Wunderlich, *Nat. Nanotechnol.* **11**, 231 (2016).
- [18] X. Marti, I. Fina, and T. Jungwirth, *IEEE T. Magn.* **51**, 2900104 (2015).
- [19] Y. A. Soh and R. K. Kummamuru, *Philos. T. R. Soc. A* **369**, 3646 (2011).
- [20] J. Basset, A. Sharma, Z. Wei, J. Bass, and M. Tsoi, *Spintronics* **7036**, 3605 (2008).
- [21] S. M. Rezende, R. L. Rodríguez-Suárez, and A. Azevedo, *Phys. Rev. B* **93**, 054412 (2016).
- [22] D. Grundler, *Nat. Nanotechnol.* **11**, 407 (2016).
- [23] L. Frangou, S. Oyarzun, S. Auffret, L. Vila, S. Gambarelli, and V. Baltz, *Phys. Rev. Lett.* **116**, 077203 (2016).
- [24] P. Wadley<sup>1</sup>, B. Howells, J. Železný, C. Andrews, V. Hills, R. P. Campion, V. Novák, K. Olejník, F. Maccherozzi, S. S. Dhesi, S. Y. Martin, T. Wagner, J. Wunderlich, F. Freimuth, Y. Mokrousov, J. Kuneš, J. S. Chauhan, M. J. Grzybowski, A. W. Rushforth, K. W. Edmonds, B. L. Gallagher, and T. Jungwirth, *Science* **351**, 587 (2016).
- [25] E. Arenholz, G. van der Laan, R. V. Chopdekar, and Y. Suzuki, *Phys. Rev. Lett.* **98**, 197201 (2007).
- [26] F. Pielmeier and F. J. Giessibl, *Phys. Rev. Lett.* **110**, 266101 (2013).
- [27] K. Kurosawa, M. Miura, and S. Saito, *J. Phys. C Solid. State.* **13**, 1521 (1980).
- [28] E. Uchida, N. Fukuoka, H. Kondoh, T. Takeda, Y. Nakazumi, and T. Nagamiya, *J. Phys. Soc. Jpn.* **23**, 1197 (1967).
- [29] L. C. Bartel and B. Morosin, *Phys. Rev. B* **3**, 1039 (1971).
- [30] I. Sanger, V. V. Pavlov, M. Bayer, and M. Fiebig, *Phys. Rev. B* **74**, 144401 (2006).
- [31] W. L. Roth, *J. Appl. Phys.* **31**, 2000 (1960).
- [32] F. Keffer and W. Osullivan, *Phys. Rev.* **108**, 637 (1957).
- [33] D. Spanke, V. Solinus, D. Knabben, F. U. Hillebrecht, F. Ciccacci, L. Gregoratti, and M. Marsi, *Phys. Rev. B* **58**, 5201 (1998).
- [34] H. Ohldag, A. Scholl, F. Nolting, S. Anders, F. U. Hillebrecht, and J. Stohr, *Phys. Rev. Lett.* **86**, 2878 (2001).
- [35] A. P. Malozemoff, *Phys. Rev. B* **35**, 3679 (1987).
- [36] X. Y. Xu, Y. J. Gao, Y. L. Wang, and J. G. Hu, *Solid State Commun.* **151**, 952 (2011).
- [37] N. C. Koon, *Phys. Rev. Lett.* **78**, 4865 (1997).
- [38] M. Wei, M. Li, Y. Zhu, M. Zhao, Q. Wang, F. Zhang, Y. Zhang, Z. Hu, R. Jiang, and D. Zhao, *J. Alloy Compd.* **676**, 96 (2016).